

**Molecular modeling of interaction between lipid monolayer and graphene
nanosheets: implications to pulmonary nanotoxicity and pulmonary drug
delivery**

Tongtao Yue,^a Xiaojuan Wang,^a Xianren Zhang,^b and Fang Huang ^{*a}

^a *State Key Laboratory of Heavy Oil Processing, Center for Bioengineering and Biotechnology, China University of Petroleum (East China), Qingdao, 266580, People's Republic of China. E-mail: fhuang@upc.edu.cn; Fax: +86-532-86981560; Tel.: +86-532-86981560*

^b *State Key Laboratory of Organic-Inorganic Composites, Beijing University of Chemical Technology, Beijing, 100029, People's Republic of China.*

The On-line Electronic Supplementary Information (ESI) includes four videos and eight figures:

Video S1: Pulmonary internalization of hydrophobic GN via direct translocation across the pulmonary surfactant monolayer.

Video S2: Pulmonary externalization of hydrophobic GN via direct translocation across the pulmonary surfactant monolayer.

Video S3: Effect of initial orientation of GN on the translocation across the pulmonary surfactant monolayer.

Video S4: Pulmonary externalization of hydrophilic GN via direct translocation

across the pulmonary surfactant monolayer.

Figure S1. Monolayer buckling and collapse of pure DPPC monolayer in the absence of GNs. The lateral pressure is fixed to $P = 3$ bar.

Figure S2. Extended MD simulations of restraining effect of hydrophilic GN on morphology transformation of DPPC monolayer.

Figure S3. Extended MD simulations of restraining effect of four hydrophilic GNs on morphology transformation of DPPC monolayer.

Figure S4. Mechanical properties of DPPC lipid monolayer. The surface tension of the monolayer increases linearly with the projected area per lipid. The GN edge length is set to $L = 5.5$ nm (black), 11 nm (red), and 16.5 nm (blue), respectively. B shows the average area compressibility modulus as a function of GN size.

Figure S5. Effect of GN thickness on the interaction with PSM.

Figure S6. Monolayer buckling and collapse in the presence of hydrophobic GN. Here the PME was used to treat the electrostatic interaction.

Figure S7. Pulmonary internalization of hydrophobic GN by translocation across the monolayer. The GN is set to keep perpendicular with the monolayer during the simulation.

Figure S8. Pulmonary internalization of hydrophobic GN via translocation across the monolayer. The pulling rate is further decreased to 0.00002 nm/ps.

Figure S9. Pulmonary internalization of hydrophilic GN by translocation across the monolayer. The GN is set to initially parallel with the monolayer.

Figure S10. Pulmonary internalization of hydrophilic GN by translocation across the

monolayer. The GN is set to keep perpendicular with the monolayer.

Figure S11. Pulmonary internalization of hydrophilic GN by translocation across the monolayer. The pulling rate is further decreased to 0.00002 nm/ps.

Figure S12. Pulmonary externalization of hydrophobic GN by translocation across the monolayer. The GN is set to initially perpendicular with the monolayer.

Figure S13. Pulmonary externalization of hydrophilic GN by translocation across the monolayer. The GN is set to initially perpendicular with the monolayer.

Figure S14. Pulmonary externalization of hydrophilic GN by translocation across the monolayer. The GN is set to initially parallel with the monolayer.

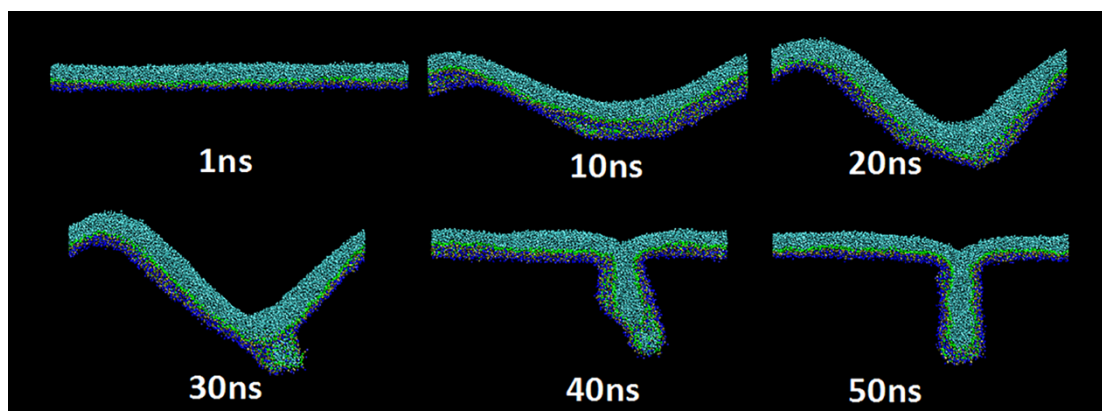


Figure S1. Monolayer buckling and collapse of pure DPPC monolayer in the absence of GNs. The lateral pressure is fixed to $P = 3$ bar.

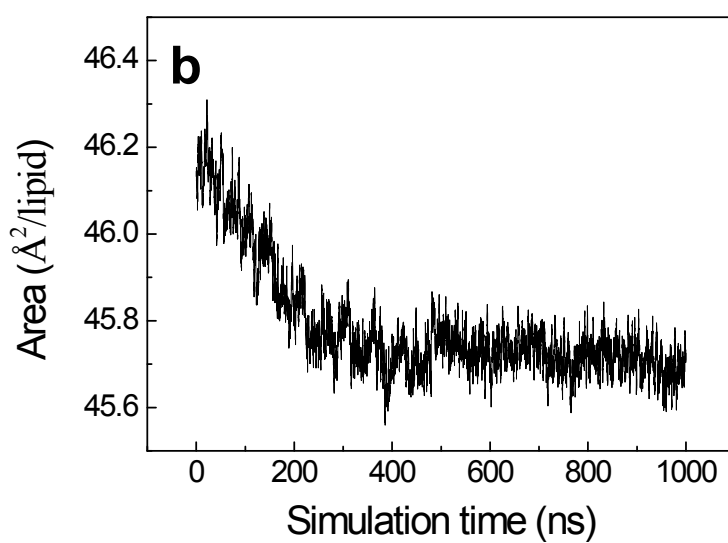
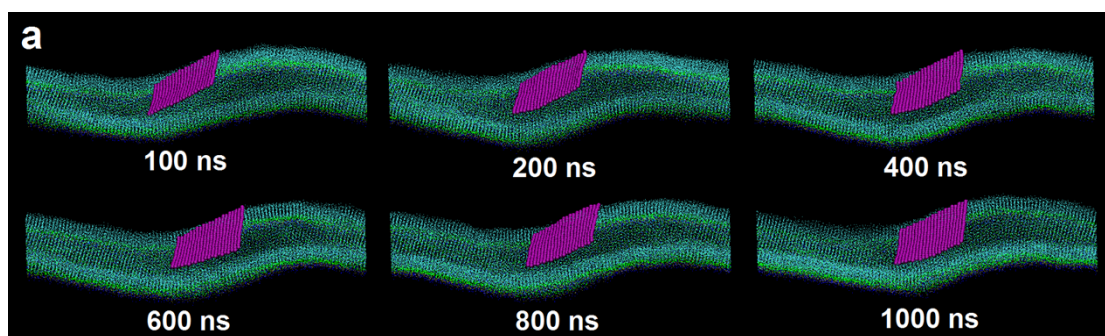


Figure S2. Extended MD simulations of restraining effect of hydrophilic GN on morphology transformation of DPPC monolayer. The lateral pressure is fixed to $P = 3$ bar, under which a monolayer-bilayer transformation occurs in the absence of GN (Fig. S1). a shows the typical snapshots and b shows the time evolution of average area per lipid.

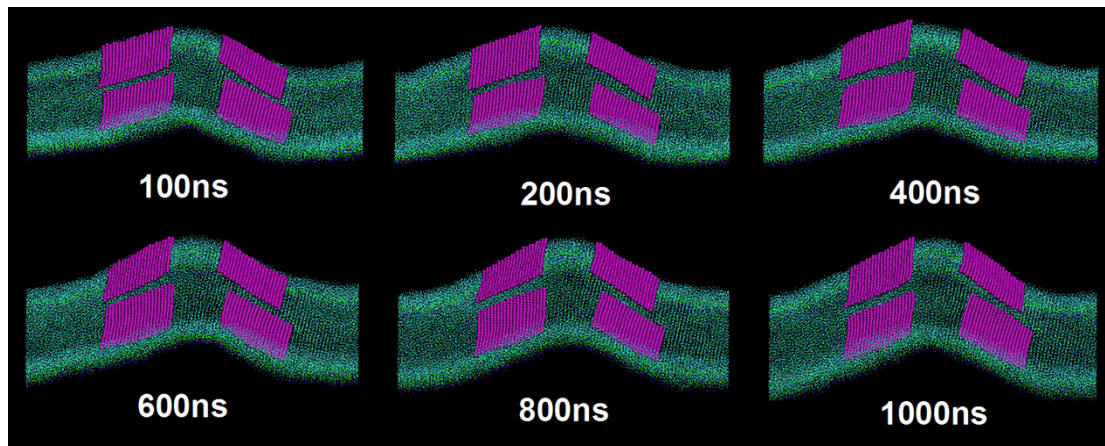


Figure S3. Extended MD simulations of restraining effect of four hydrophilic GNs on morphology transformation of DPPC monolayer. The lateral pressure is fixed to $P = 5$ bar, under which a monolayer-bilayer transformation occurs in the present of one hydrophilic GN (Fig. 5).

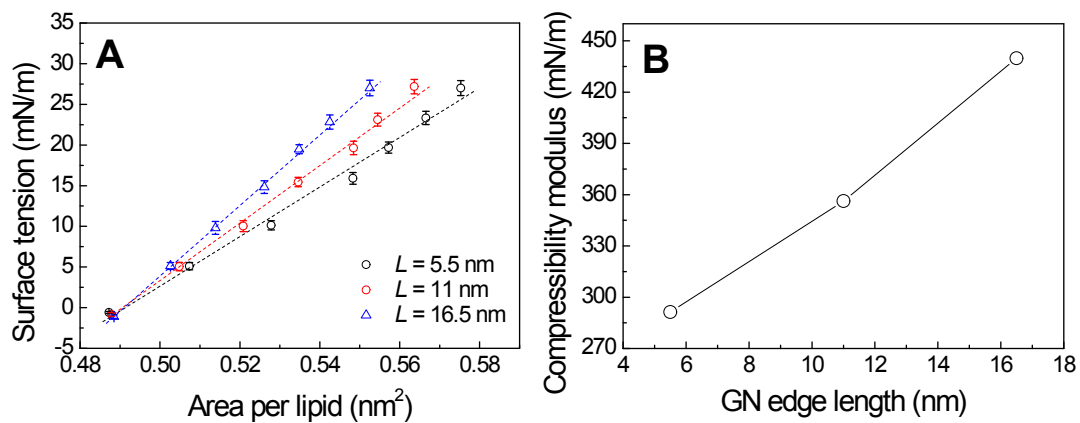


Figure S4. Mechanical properties of DPPC lipid monolayer. The surface tension of the monolayer increases linearly with the projected area per lipid. The GN edge length is set to $L = 5.5$ nm (black), 11 nm (red), and 16.5 nm (blue), respectively. B shows the average area compressibility modulus as a function of GN size.

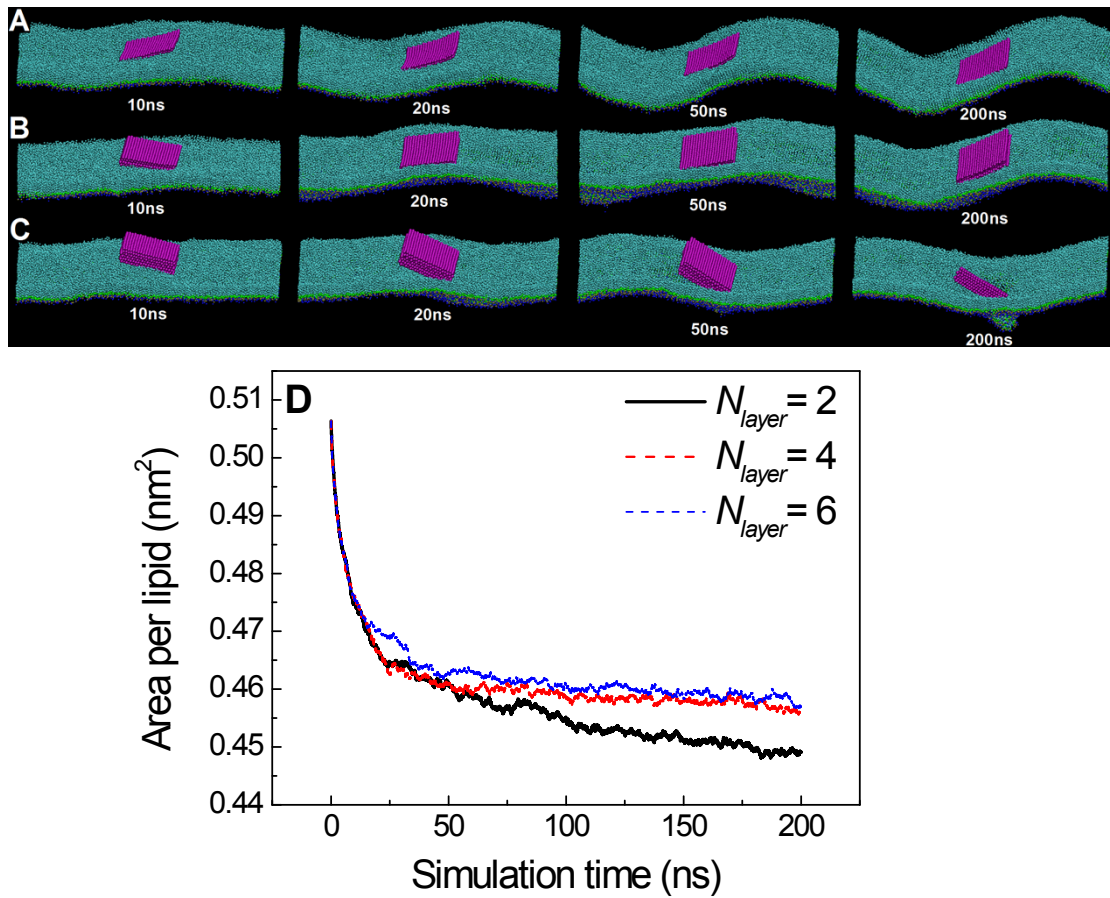


Figure S5. Effect of GN thickness on the interaction with PSM. A-C shows the typical snapshots of interaction between PSM and hydrophilic GNs with different thicknesses (A: $N_{layer} = 2$; B: $N_{layer} = 4$; C: $N_{layer} = 6$). D shows the time evolution of area per lipid.

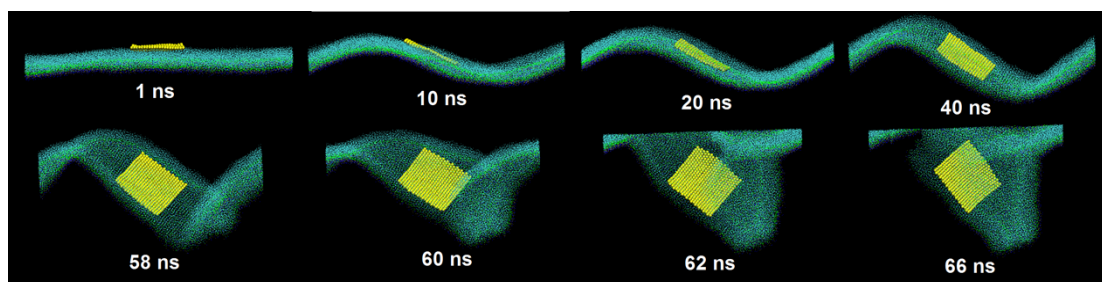


Figure S6. Monolayer buckling and collapse in the presence of hydrophobic GN. Here the PME was used to treat the electrostatic interaction.

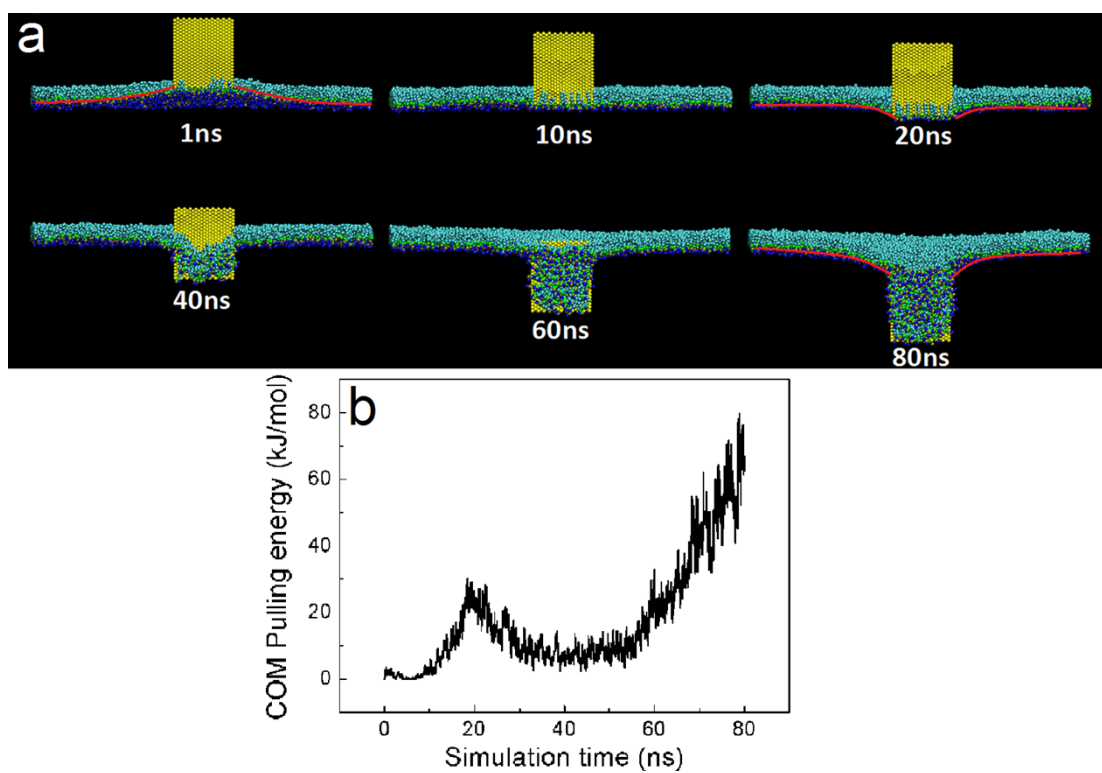


Figure S7. Pulmonary internalization of hydrophobic GN by translocation across the monolayer. The GN is set to keep perpendicular with the monolayer during the simulation. a shows the typical snapshots, b shows the time evolution of COM pulling energy. The red line indicate the local monolayer deformation during the translocation process.

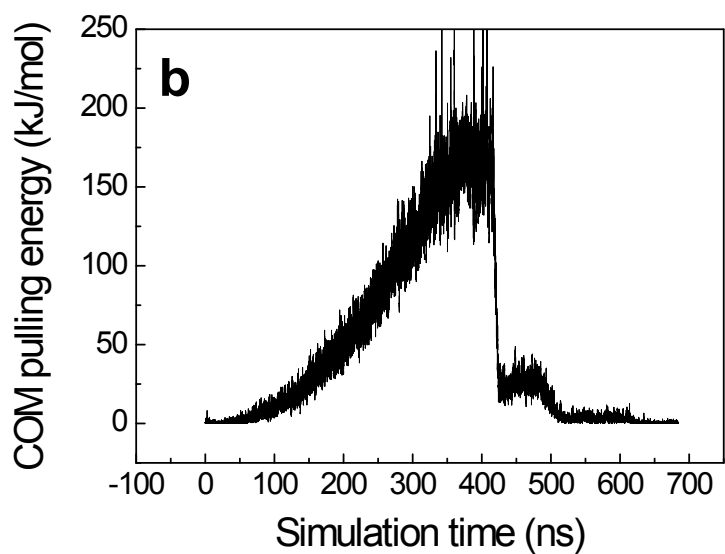
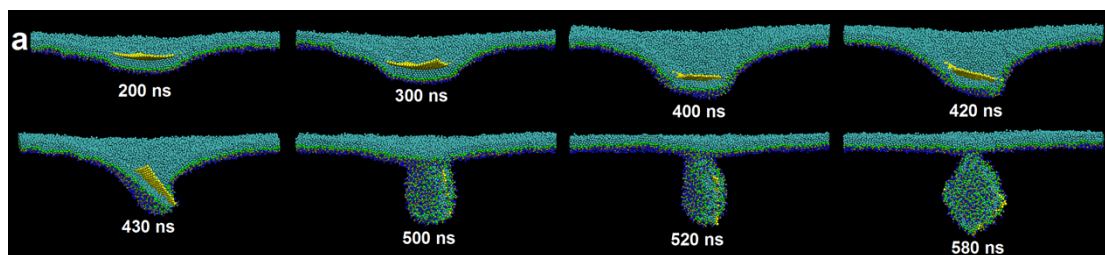


Figure S8. Pulmonary internalization of hydrophobic GN via translocation across the monolayer. The pulling rate is further decreased to 0.00002 nm/ps. The GN is placed initially in the air phase and is parallel with the monolayer. a shows the typical snapshots and b shows the time evolution of COM pulling energy.

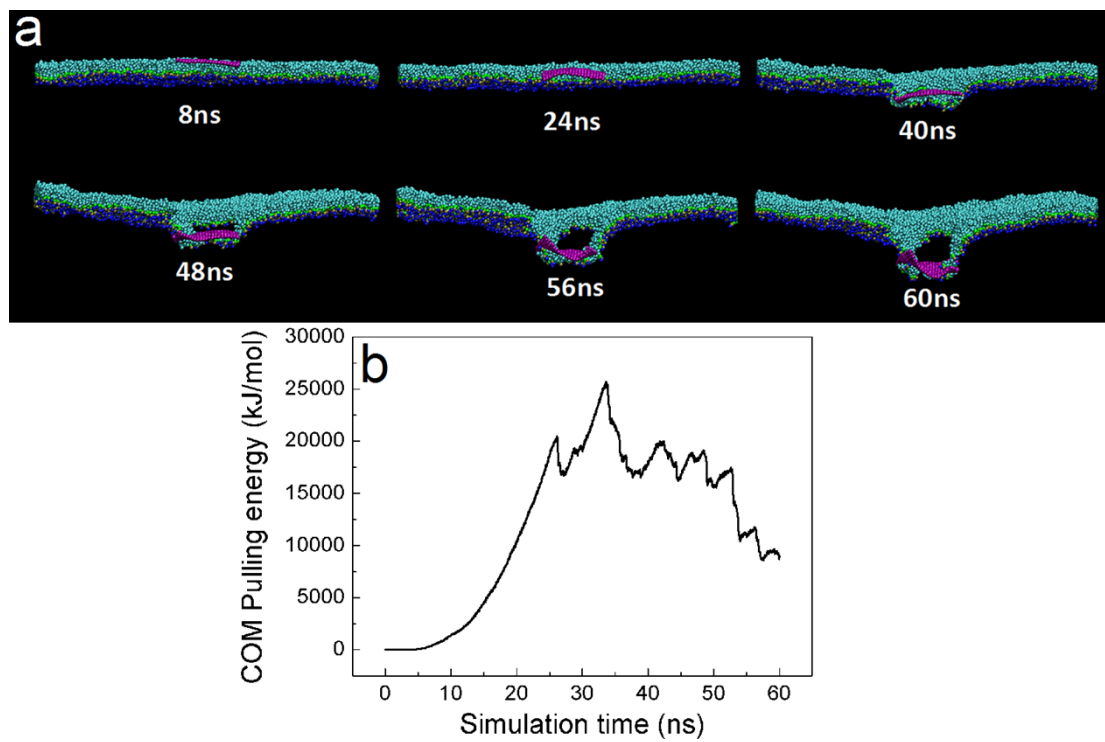


Figure S9. Pulmonary internalization of hydrophilic GN by translocation across the monolayer. The GN is set to initially parallel with the monolayer. a shows the typical snapshots, and b shows the time evolution of COM pulling energy.

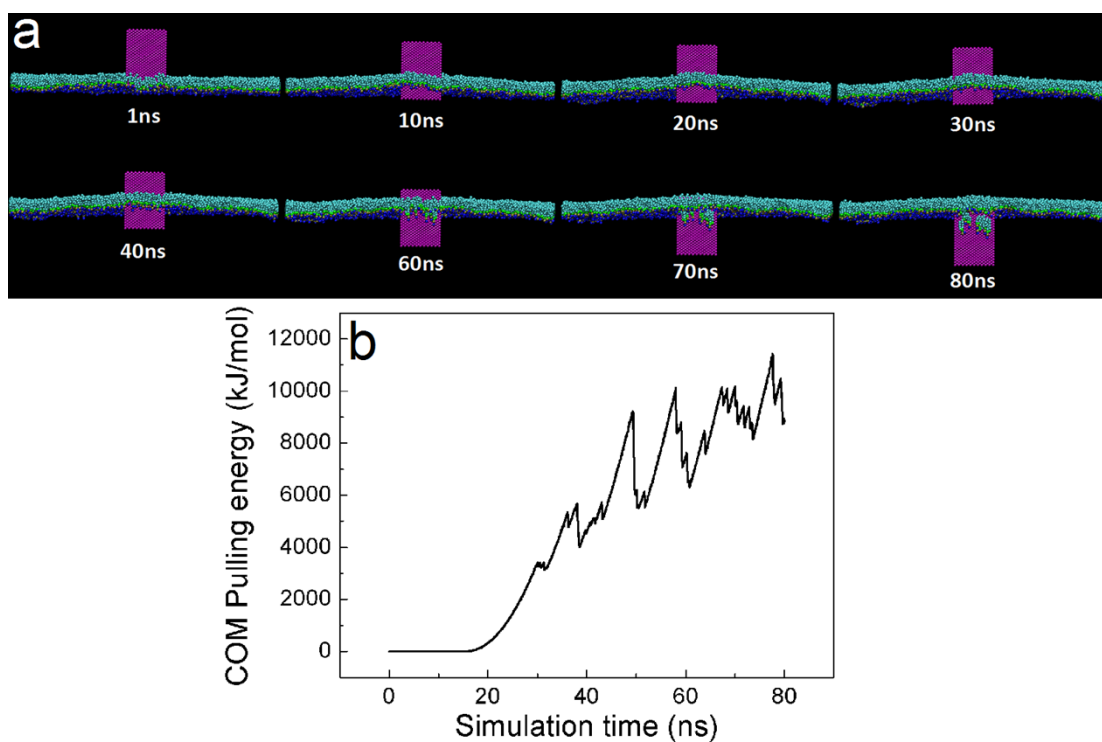


Figure S10. Pulmonary internalization of hydrophilic GN by translocation across the monolayer. The GN is set to keep perpendicular with the monolayer. a shows the typical snapshots, and b shows the time evolution of COM pulling energy.

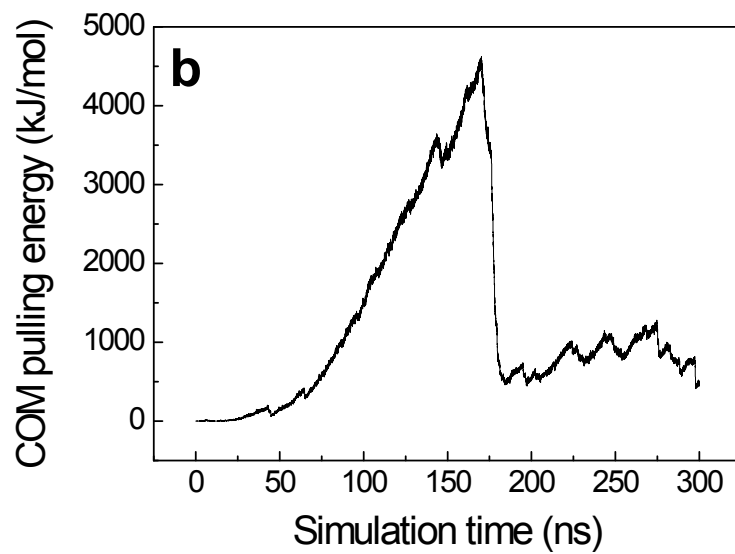
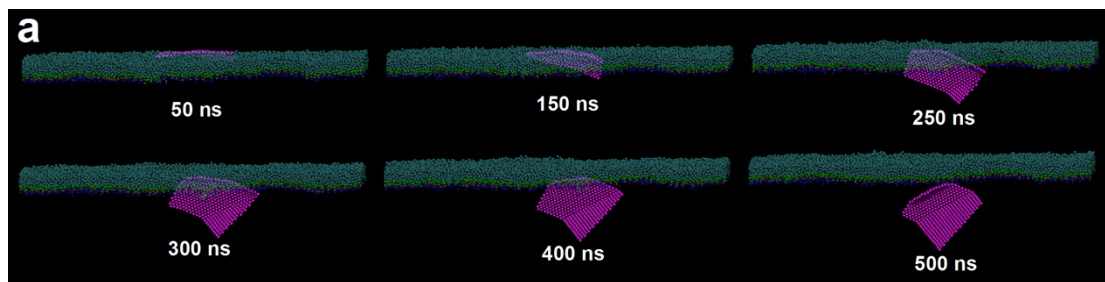


Figure S11. Pulmonary internalization of hydrophilic GN by translocation across the monolayer. The pulling rate is further decreased to 0.00002 nm/ps. a shows the typical snapshots, and b shows the time evolution of COM pulling energy.

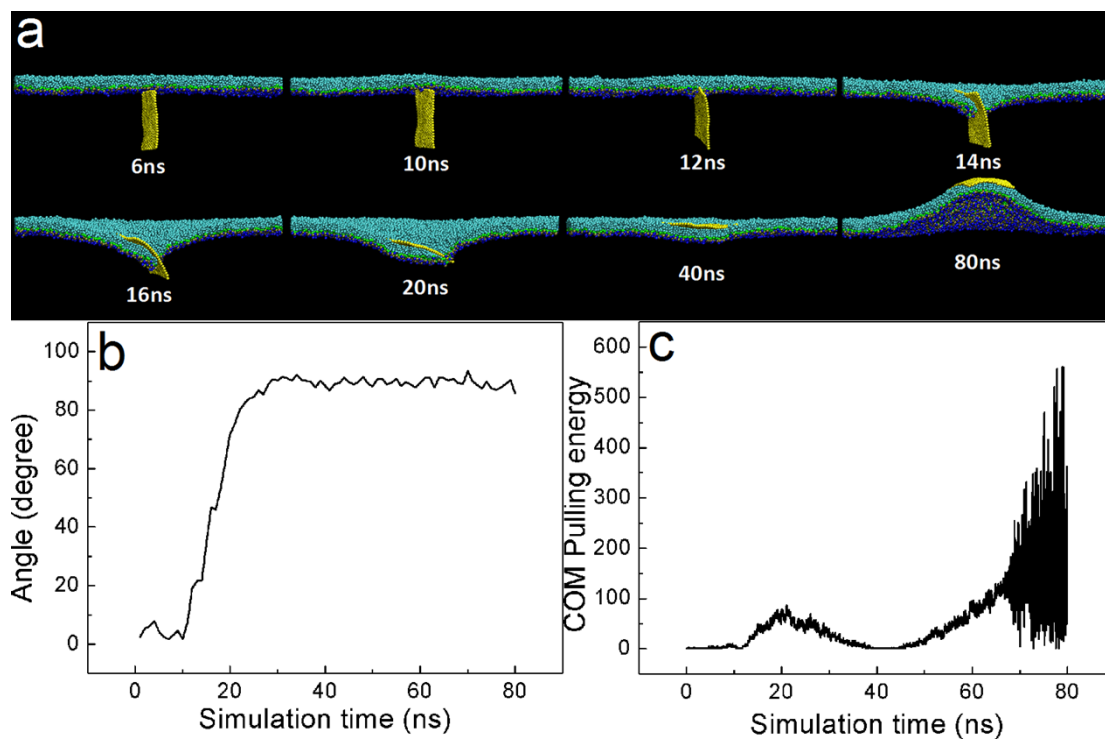


Figure S12. Pulmonary externalization of hydrophobic GN by translocation across the monolayer. The GN is set to initially perpendicular with the monolayer. a shows the typical snapshots, b shows the time evolution of angle between GN and membrane normal, and c shows the time evolution of COM pulling energy.

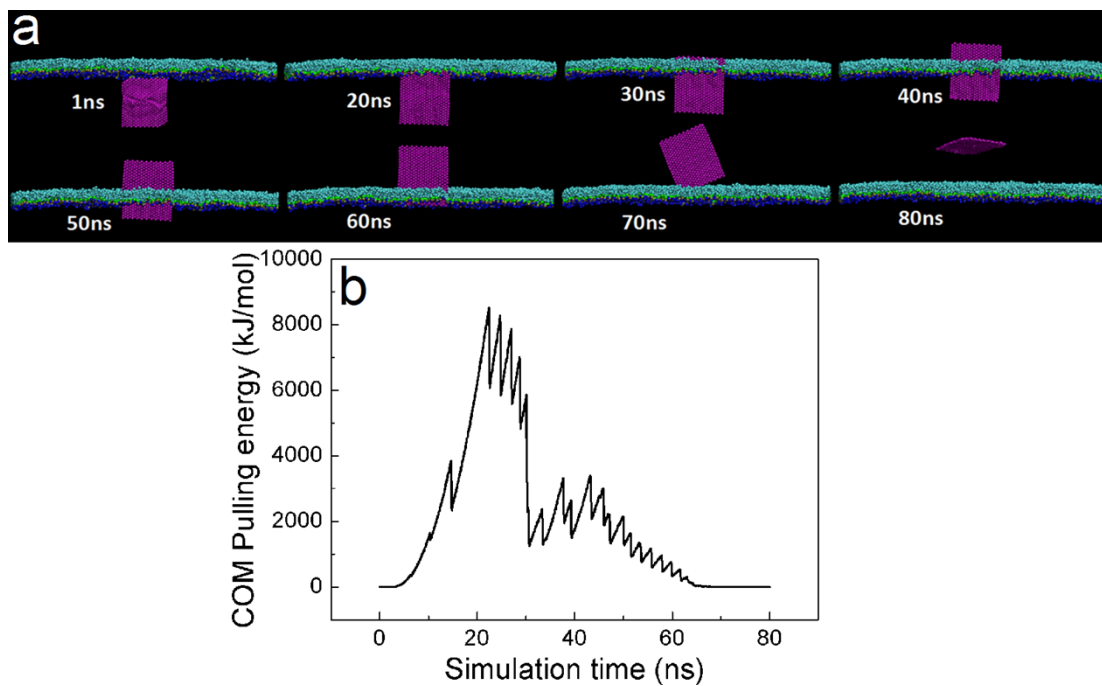


Figure S13. Pulmonary externalization of hydrophilic GN by translocation across the monolayer. The GN is set to initially perpendicular with the monolayer. a shows the typical snapshots, and b shows the time evolution of COM pull energy.

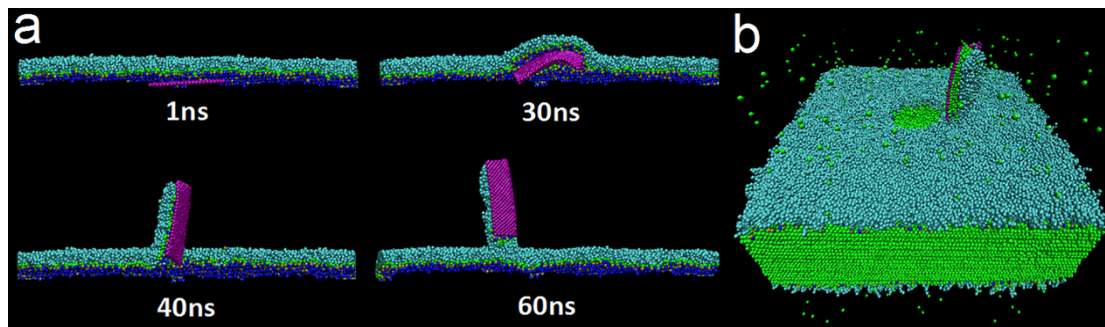


Figure S14. Pulmonary externalization of hydrophilic GN by translocation across the monolayer. The GN is set to initially parallel with the monolayer. a shows the typical snapshots, and b shows the final snapshot from which we can see the monolayer rupture stretched by the GN.